Assessing the Performance of NOMA in a Multi-Cell Context: A General Evaluation Framework

Anthony Bardou, Jean-Marie Gorce, *Senior Member, IEEE*, and Thomas Begin

***Abstract*—Non-Orthogonal Multiple Access (NOMA) is a Resource Sharing Mechanism (RSM) initially studied for 5G cellular networks and brought back to the agenda for 6G networks. While NOMA's benefit at the level of a single cell has been properly established, assessing its performance at the scale of a cellular network remains an open research problem. This is mainly due to the inter-dependencies between scheduling, power control and inter-cell interference. Some algorithms have been proposed to optimize resource allocation in a multi-cell network, but they require a perfect and unrealistic knowledge of the whole channel states. In this paper, we leverage Bayesian Optimization techniques to build a versatile evaluation framework, able to assess the performance of multi-cell networks implementing a large variety of RSMs under a minimal set of assumptions. Subsequently, we illustrate how this evaluation framework can be used to compare the performance of several well-known RSMs under various fairness requirements and beamforming efficiencies. Our results show that, among the RSMs studied on a simple multi-cell network simulation, NOMA combined with a full reuse policy consistently emerges as the one able to achieve the highest end-users achievable rates under fairness constraints.**

***Index Terms*—Cellular networks, NOMA, Bayesian optimization, fairness.**

I. Introduction

SHARING radio resources is a key problem in cellular networks since their infancy. Inside each cell, multiple access techniques exploit orthogonal resources (in time, frequency, or codes) while inter-cell interference (ICI) is controlled through sophisticated reuse policies. Typically, for second-generation (2G) cellular networks, ICI was controlled through static resource allocation based on graph coloring. For third generation (3G) cellular networks, ICI was mitigated by the use of scrambling codes and by controlling the load factor of the cells. For fourth generation (4G) cellular networks exploiting Orthogonal Frequency-Division Multiple Access (OFDMA), graph coloring strategies were enhanced with fractional frequency reuse (FFR) [1], [2], [3] or even full-reuse policies [4]. Indeed, if graph coloring-based approaches provide high signal-to-interference-plus-noise-ratio (SINR) to edge users, they suffer from a strong reduction of the frequency bandwidth available for each cell. Conversely, full reuse consists in providing each cell with the full bandwidth in spite of the potential high interference generated for edge users. Full reuse has been shown to provide a higher network spectral efficiency despite the low SINR associated with edge users (typically below 0 dB). FFR was elaborated as a tradeoff between both strategies, by considering the superposition of two classes of users: inner users in the center of the cell, and edge users, whose reuse strategy differs. Inner users exploit a fraction of the spectrum in a full reuse scheme whereas a graph coloring strategy on the remainder of the spectrum is applied for edge users [2], [3].

During the elaboration of the fifth generation (5G), enhancing 4G capabilities, resource-sharing strategies based on non-orthogonal multiple access (NOMA) techniques have been extensively investigated [5], [6]. NOMA is a powerful technique that has the potential to increase the multiple access cellular network capacity [7] both in the downlink and the uplink. NOMA relies on the well-known principle of superposition coding (SC) elaborated for the Gaussian broadcast channel (G-BC) where two (or more) data streams are superposed [8]. In a 2-user NOMA, pairing a strong and a weak user together (with respect to their channel quality) greatly increases the cell's capacity. In such a setup, and unlike orthogonal multiple access (OMA), NOMA achieves the Shannon capacity region bounds for the G-BC. The expression of this capacity for a single cell under massive access is provided in [9] and shows the benefit of NOMA approaches even with dealing with a limited number of superposed data streams.

While NOMA has been shown to be a powerful strategy at the scale of a single cell, its benefits at the scale of a full network are not straightforward to establish. In particular, its impact on the ICI and on the optimal User Equipment (UE)-Base Station (BS) association has not yet been precisely evaluated. In [10], the authors analyzed the disincentives for the use of NOMA in 5G, and raised a few common myths about NOMA, showing that: (i) NOMA can achieve a good tradeoff between spectral efficiency and fairness; (ii) NOMA is not very complex to implement, at least when restricted to the superposition of pairwise users; (iii) NOMA can be combined with FFR strategies (contrary to a previous statement [11]).

Received 19 July 2024; revised 6 February 2025 and 28 May 2025; accepted 23 June 2025. Date of publication 11 July 2025; date of current version 22 December 2025.The associate editor coordinating the review of this article and approving it for publication was K. Tourki. *(Corresponding author: Anthony Bardou.)*

Anthony Bardou is with IC, EPFL, 1015 Lausanne, Switzerland (e-mail: anthony.bardou@epfl.ch).

Jean-Marie Gorce is with INSA Lyon, Inria, CITI, 69100 Villeurbanne, France.

Thomas Begin is with ENS Lyon, CNRS, LIP, University Lyon 1, 69000 Lyon, France.

Digital Object Identifier 10.1109/TWC.2025.3584178

Because of these observations, optimizing non-orthogonal resource-sharing mechanisms (RSMs) at the scale of a network is a complex matter. However, if the transmission power levels of each BS and the UE-BS associations are efficiently optimized, then NOMA can let the cells breathe, thus bringing more flexibility than classical intra-cell optimization while remaining less complex than a cell-free approach as currently investigated for sixth generation (6G) cellular networks [12]. This is why NOMA is still under evaluation for 6G [13].

However, the integration of NOMA in the future 6G cellular networks requires firstly evidence that its benefit at the system level is significant, and, secondly that realistic RSMs algorithms and protocols can be developed. The first challenge is inherently difficult as it depends on complex optimization problems, as highligthed in [14] and [15].

The second challenge concerns the development of distributed RSMs algorithms that takes into account exact channel realizations, channel state estimation, codes and instantaneous performances. This line of research is very active and several algorithms have been proposed [11], [16], [17], [18], [19], [20], [21], [22], [23], [24], [25]. However the performance metrics obtained in these references heavily depend on the technical choices and the simulation parameters, making difficult to understand the specific benefit of NOMA.

In this context, our paper focuses on the first challenge and proposes a general evaluation framework to assess the performance of an arbitrary RSM in a multi-cell context.

In essence, this framework aims to optimize the parameters of a cellular network implementing the RSM under evaluation before collecting the RSM's performance metrics. The framework formulates the optimization of the cellular network as a black-box optimization problem. This makes our framework versatile, as it is able to find efficient configurations in the cellular network under a minimal set of assumptions (e.g., regardless of the actual network topology or the interference model in use). Then, we apply this framework to compare the respective performance of several existing RSMs on a simulated, real-life-inspired cellular network. Our results tend to show the superiority of NOMA (used in conjunction with a full reuse policy) at finding the best tradeoffs between high UEs rates, under various fairness requirements and beamforming efficiencies.

It is worth noting that this paper does not propose an RSM algorithm like those mentioned above [11], [16], [17], [18], [19], [20], [21], [22], [23], [24], [25]. Our reasoning is closer to the papers based on stochastic geometry, following the seminal paper of Andrews et al. [26] that provides system-level performance bounds.

The remainder of the paper is organized as follows. Section II describes the methods previously proposed to evaluate NOMA in a multi-cell context and motivates the need for a general, agnostic evaluation framework for RSMs. Section III introduces the optimization framework and its parameters. Section IV describes the framework parameters chosen for the conducted study. Section V illustrates the abilities of the framework by comparing the performance of several RSMs and provides insights on the performance of NOMA at the cellular network scale. Finally, Section VI concludes the paper.

II. NOMA-Based Resource-Sharing Evaluation

Evaluating NOMA at the scale of a network is an important but hard problem if we consider simultaneously power transmission levels, UE-BS association, and NOMA encoding ordering. In this paper, we consider power-domain NOMA that we simply refer to as NOMA for the sake of brevity.

In [16] and more recently in [19], algorithmic solutions for sum-power minimization - sum-rate maximization for multi-cell networks with NOMA are investigated. In these papers, the UE-BS association is fixed, and the proposed algorithms jointly optimize the resource and power allocation to each UE. The proposed strategies rely on a multi-level NOMA over multiple resource blocks. The proposed approaches leverage the multiple degrees of freedom brought by NOMA. However, in practice, these solutions would require a huge amount of signaling between all UEs and BSs, making their implementation challenging. In [17], an optimal algorithm is studied for NOMA allocation in a single cell, on multiple sub-bands, with a weighted sum-rate. This cost function may include some notion of fairness, but the choice of individual weights is complex. A less complex algorithm is proposed by the same authors in [18]. In [20], advanced algorithms are proposed for pure NOMA and mixed strategies in a single cell configuration. These solutions are extended in [21] to multi-cells and is complementary to [11]. Both contributions proposed an optimization of UEs association, power and SIC ordering in the multi-cell network considering an effective algorithm (and not to evaluate and compare RSMs techniques as is the case of our paper). Among new RSMs algorithms, it is worth mentioning [22], [25] that explore NOMA massive access in the uplink as well as [23] and [24] that use online algorithms and leverage mobile edge computing.

In [27], the authors combine FFR and NOMA. They consider a classical FFR and they superpose, on top of it, a third category of UEs with low power. Unfortunately, this scheme induces a higher complexity and does not prevent the loss of performance already observed for FFR.

Another avenue to evaluate cellular networks is stochastic geometry [26]. Based on spatial randomness, this powerful analytical tool enables the computation of the distribution of BS/UE radio links' quality (e.g., rate or outage). Stochastic geometry has been used to evaluate the impact of FFR mechanisms with OFDMA in [28] and [29]. However, modeling NOMA in multi-cell was fully achieved, due to the complexity of modeling SIC with random distribution of UEs. In [30], the authors studied NOMA at a large scale but their results were limited to SINR meta-distributions. The authors were able to evaluate individual rates of UEs but not a global evaluation of the sum-rates, as this would require the distribution of the cell geometry as discussed in [31], which is generally hard to determine. The more advanced contributions are [32] for the uplink with Coordinated Multi-Point (COMP), [33] in cell-free mode, or [34] which considers a scenario close to ours but focuses on the coverage probability, which does not allow the computation of the overall system capacity and UE individual rates.

The majority of existing studies focus on evaluating the performance of a specific RSM under particular scenarios and assumptions. However, even if all these approaches were implemented, comparing the relative performance of different RSMs would remain challenging due to the varying assumptions and constraints in each study. In this paper, we introduce a general framework that leverages the flexibility of Bayesian Optimization (BO) to accommodate nearly all existing RSMs within arbitrary cellular networks comprising multiple cells. This unified framework ensures a fair and consistent comparison of the evaluated RSMs.

III. Unified Framework for the Evaluation of RSMs

A. Core Idea

To accurately assess the performance of any RSM for a cellular network, it is essential to operate the RSM under its optimal parameter configuration. Therefore, our evaluation framework must be capable of optimizing the parameters of existing RSMs, allowing a fair comparison of their respective merits. That is why, at the core of the proposed evaluation framework lies the following optimization problem:

$$\underset{\boldsymbol{x}\in\mathcal{D}}{\text{maximize}}\, f(\boldsymbol{x};\mathcal{T},\mathcal{P},\mathcal{R}). \tag{1}$$

The problem (1) comprises five core ingredients:

- the RSM $\mathcal{R}$ to evaluate (e.g., NOMA)
- the propagation model $\mathcal{P}$ (e.g., log-distance path loss, accounting for beamforming, shadowing...),
- the cellular network topology $\mathcal{T}$,
- the network parameters to optimize (e.g., the power levels of the BSs), specified by a search space $\mathcal{D}$,
- a scalar objective function $f : \mathcal{D} \to \mathbb{R}$ collecting the performance of the cellular network specified by the triplet $(\mathcal{T},\mathcal{P},\mathcal{R})$ and parameterized by $\boldsymbol{x} \in \mathcal{D}$.

These five ingredients are typically set by the performance analyst and, together, they specify our optimization problem (1). The goal of the evaluation framework is to solve (1) by discovering $\boldsymbol{x}^* = \arg\max_{\boldsymbol{x}\in\mathcal{D}} f(\boldsymbol{x})$[1] (note that the parameters $\mathcal{T}$, $\mathcal{P}$ and $\mathcal{R}$ have been omitted for the sake of brevity) with the procedure explained in the next section. Finally, once the cellular network is adequately configured for the RSM $\mathcal{R}$, key performance metrics can be collected and sent to the performance analyst. Following this procedure for every RSM $\mathcal{R}$, the evaluation framework ensures that the same performance metric f is optimized with the same algorithm $\mathcal{A}$ by tuning the same cellular network parameters $\boldsymbol{x}$, successfully avoiding the inconsistencies in RSMs evaluations raised in Section II.

B. Bayesian Optimization

Optimizing the objective function f in (1) is generally a challenging task. The ingredients $\mathcal{D},\mathcal{T},\mathcal{P}$ and $\mathcal{R}$ can have complex, intricate, non-convex effects on the objective function f, making higher-order information (e.g., gradient $\nabla_{\boldsymbol{x}} f$, Hessian $\nabla^2_{\boldsymbol{x}} f$, where ∇ denotes the vector differential operator, also known as del) unavailable. Additionally, the lack of a comprehensive, diverse and representative dataset mapping the network parameters and the performance metrics prevents the use of offline machine learning models (e.g., neural networks). Therefore, f can be treated as a black-box function, which must be optimized in an online manner, where it is simulatenously discovered and optimized. Due to the black-box nature of f, traditional first-order optimization methods such as gradient descent [35] are not applicable to the problem (1). Since f is computed by collecting performance metrics on the cellular network, it can also be considered expensive to evaluate and noisy. Therefore, higher-order information cannot be approximated by Monte-Carlo-based estimators [36]. In this context, BO appears as a natural candidate to solve (1), as this framework has been successfully applied to many black-box optimization problems in a variety of domains [37], [38], [39]. In this section, we provide some background about BO and introduce its core assumption.

A BO algorithm often leverages a Gaussian process (GP) as a surrogate model [40] for the black-box objective function f. A GP is a stochastic process, that is, a collection of random variables $\{Y(\boldsymbol{x})\}_{\boldsymbol{x}\in\mathcal{D}}$ indexed by a set $\mathcal{D}$. As its name suggests, in a GP, any finite collection $\{Y(\boldsymbol{x}_1),\cdots,Y(\boldsymbol{x}_k)\}$ has a joint multivariate Gaussian distribution. As such, it is fully specified by its mean function $\mu(\boldsymbol{x}) = \mathbb{E}[Y(\boldsymbol{x})]$ (we assume $\mu(\boldsymbol{x}) = 0$ without loss of generality) and its covariance function $k(\boldsymbol{x},\boldsymbol{x}') = \mathbb{E}[(Y(\boldsymbol{x}) - \mu(\boldsymbol{x}))(Y(\boldsymbol{x}') - \mu(\boldsymbol{x}'))]$.

For the objective function f to be reasonably modeled by a GP, it only needs to be continuous. In fact, it is known that any continuous scalar function on a compact subset of $\mathbb{R}^d$ can be approximated arbitrarily well by a GP posterior mean for some covariance functions k. For more details, please refer to [41].

As mentioned above, the versatility of the GP as a surrogate model heavily relies on its covariance function k. In fact, a GP can be a satisfying model for rough functions (e.g., by setting k so that the GP is a Ornstein-Uhlenbeck process [42]) as well as smooth ones (e.g., by setting k to be a Radial Basis Function kernel [43]). Covariance functions can also be combined with basic operators (e.g., summed or multiplied) to form richer covariance functions that encode complex correlations between objective function values.

Let $\boldsymbol{X}_t = (\boldsymbol{x}_1,\cdots,\boldsymbol{x}_t)$ be a $t \times d$ matrix of inputs (*i.e.*, t inputs of d dimensions) and $\boldsymbol{y}_t = (f(\boldsymbol{x}_1)+\epsilon,\cdots,f(\boldsymbol{x}_t)+\epsilon)$ be a corresponding t-dimensional vector of observed noisy outputs, with $\epsilon \sim \mathcal{N}(0,\sigma^2)$. Then, if f is a GP, $f(\boldsymbol{x})|\boldsymbol{X}_t,\boldsymbol{y}_t \sim \mathcal{N}\left(\mu_t(\boldsymbol{x}),\sigma_t^2(\boldsymbol{x})\right)$ with

$$\mu_t(\boldsymbol{x}) = \boldsymbol{k}^\top(\boldsymbol{x},\boldsymbol{X}_t)\boldsymbol{\Delta}_t^{-1}\boldsymbol{y}_t, \tag{2}$$

$$\sigma_t^2(\boldsymbol{x}) = k(\boldsymbol{x},\boldsymbol{x}) - \boldsymbol{k}^\top(\boldsymbol{x},\boldsymbol{X}_t)\boldsymbol{\Delta}_t^{-1}\boldsymbol{k}(\boldsymbol{x},\boldsymbol{X}_t) \tag{3}$$

where $\boldsymbol{k}(\boldsymbol{x},\boldsymbol{X}_t) = (k(\boldsymbol{x},\boldsymbol{x}_i))_{i\in[1,t]}$, $\boldsymbol{\Delta}_t = \boldsymbol{K}_t + \sigma^2\boldsymbol{I}_t$, $\boldsymbol{I}_t$ is the $t \times t$ identity matrix, $\boldsymbol{K}_t = (k(\boldsymbol{x}_i,\boldsymbol{x}_j))_{i,j\in[1,t]}$ and where $\boldsymbol{u}^\top$ denotes the transpose of $\boldsymbol{u}$.

At time t, a BO algorithm must find the next query $\boldsymbol{x}_{t+1} \in \mathcal{D}$ such that $f(\boldsymbol{x}_{t+1})$ is likely to be large, and such that observing $f(\boldsymbol{x}_{t+1})$ brings information about the

[1]In this paper, f is assumed to be scalar. We postpone the extension of the framework to vector-valued objective functions to future works.

Algorithm 1 Proposed Evaluation Framework

Input: RSM $\mathcal{R}$, propagation model $\mathcal{P}$, network topology $\mathcal{T}$, network parameters domain $\mathcal{D}$, black-box objective function f, BO algorithm $\mathcal{B}$.
Output: key performance metrics $\mathcal{M}$

$t = 0$
Initialize the datasets $\boldsymbol{X}_t = \emptyset, \boldsymbol{y}_t = \emptyset$
while $\mathcal{B}$ does not converge **do**
  Use $\mathcal{B}$ and the datasets $(\boldsymbol{X}_t, \boldsymbol{y}_t)$ to find $\boldsymbol{x}_{t+1}$
  Set the network parameters to $\boldsymbol{x}_{t+1}$
  Collect $y_{t+1} = f(\boldsymbol{x}_{t+1}) + \epsilon$ on the network
  Update the datasets $\boldsymbol{X}_{t+1} = \boldsymbol{X}_t \cup \{\boldsymbol{x}_{t+1}\}$, $\boldsymbol{y}_{t+1} = \boldsymbol{y}_t \cup \{y_{t+1}\}$
end while
Collect key performance metrics $\mathcal{M}$ on the network with optimized parameters $\boldsymbol{x}^* \in \mathcal{D}$
return: $\mathcal{M}$

black-box f. This exploration-exploitation dilemma is usually solved by maximizing an acquisition function $\varphi_t(\boldsymbol{x})$. Many acquisition functions exist, such as GP-UCB [44], Knowledge Gradient [45], Probability of Improvement [46] and Expected Improvement [47].

C. Evaluation Framework Algorithm

The proposed evaluation framework is given in Algorithm 1. As previously described, Algorithm 1 solves the optimization problem (1) with a BO algorithm $\mathcal{B}$, before collecting the key performance metrics on the optimized network and returning them to the performance analyst.

In addition to the five main ingredients described in Section III-A, the performance analyst must also provide a BO algorithm $\mathcal{B}$. In fact, depending on the problem specified by the five main ingredients of the framework, some BO algorithms may be more suited than others (e.g., high-dimensional BO algorithms [48], batch BO algorithms [49]).

In the following sections, we illustrate the capabilities of Algorithm 1 by providing valuable insights on the performance of NOMA-based RSMs. Section IV describes how the main ingredients of the framework (including the BO algorithm $\mathcal{B}$) are specified, while Section V provides and discusses the results of our study.

IV. Description of the Study

In this section, we describe how the evaluation framework proposed in Section III is used to produce key performance metrics enabling the comparison between five different RSMs. The study is conducted on a cellular network covering a service area Ω. It comprises a set of n BSs and a set of m UEs distributed over Ω. Each UE is associated with the BS that provides the highest SINR. Note that the evaluation framework presented in Section III is agnostic to the UE-BS association policy. In other words, it can be used without modification to evaluate, at the scale of a cellular network, RSMs that implements a different UE-BS association policy.

A. Resource-Sharing Mechanisms $\mathcal{R}$

In this study, we compare a set of five different RSMs that comprises both classical RSMs used in cellular networks and hybrid RSMs that combine NOMA with classical RSMs. Each of them is illustrated in Figure 1 and briefly described in the following.

The simplest studied RSM is the full reuse solution (`FR`) used for 4G networks, which does not introduce any additional mechanism to mitigate ICI. Another simple RSM is the classical graph-coloring solution (`COLORING`) used for 2G networks, which partitions the frequency band into chunks of equal size and allocates different chunks to neighboring cells. ICI is effectively mitigated, at the expense of a significant shrinkage of the frequency band available for each UE. Next, we consider the fractional frequency reuse solution (`FFR`), which introduces an additional structure within each cell by splitting it into an inner and an outer region. It allocates a chunk of size τ in the frequency band for the cells' inner regions while the cells' outer regions share the remainder of the frequency band (of size $W-\tau$) with a color-based solution.

We compare these RSMs with two NOMA-based RSMs, where each BS exploits a 2-user NOMA technique.[2] With NOMA, each cell is split into an inner and an outer region. SC is used on the two regions, and SIC is performed by the inner UEs to remove the interference due to the signals transmitted to the outer UEs. On the one hand, `NOMA+FFR` combines FFR and NOMA, following the concept proposed in [10]. The inner UEs adopt a full reuse strategy, while the outer UEs adopt a color-based strategy. On the other hand, `NOMA+FR` proposes that all UEs (inner and outer) adopt a full reuse strategy.

Note that the chosen procedure used to split a cell into an inner and an outer region is detailed in Appendix A.

B. Parameters $\mathcal{D}$ and Objective Function f

We consider a single transmission power level for each region of the cellular network. For the RSMs `FR` and `COLORING`, this naturally implies that each BS i ($i \in [1, n]$) has a single transmission power level x_i. We assume that each BS has a minimal transmission power level of P_- and a maximal transmission power level of P_+. This leads to a natural formulation for the optimization parameters $\boldsymbol{x} = (x_1, \cdots, x_n) \in \mathcal{D}$ with

$$\mathcal{D} = \mathcal{D}^{(1)} \times \cdots \times \mathcal{D}^{(n)} = [P_-, P_+]^n. \tag{4}$$

For the RSMs that split each cell into two regions, we consider two transmission power levels $\boldsymbol{p}_i = \left(p_i^{(in)}, p_i^{(out)}\right)$ per BS i, $i \in [1, n]$. Despite the relative simplicity of this scenario, one can expect a significant capacity gain [9]. In this formulation, each $\boldsymbol{p}_i$ must also satisfy a power constraint, that is $P_- \leq ||\boldsymbol{p}_i||_1 \leq P_+$, where $||\cdot||_p$ is the L^p-norm such that $||\boldsymbol{x}||_p = \left(\sum_{i=1}^n |x_i|^p\right)^{1/p}$. Furthermore, we enforce $p_i^{(in)} \leq p_i^{(out)}$. It is worth noting that our proposed framework can

[2] Although our framework imposes no theoretical limit on the number of superposition levels, previous studies have shown [9] that increasing the number of levels beyond two yields only moderate additional gains while significantly increasing the complexity of resource allocation, decoding algorithms, and the optimization process.

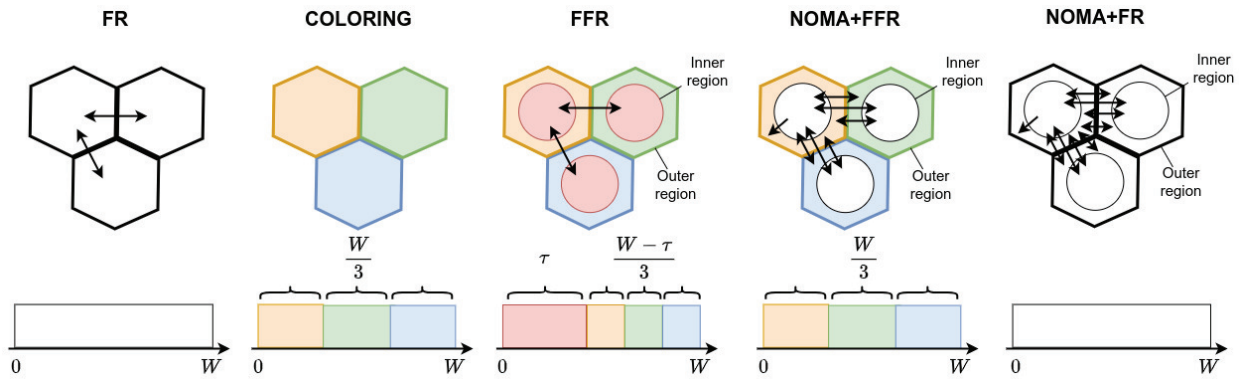

Fig. 1. The studied RSMs illustrated on three adjacent hexagonal cells and the corresponding splitting of the frequency band of size W. Interference between the top left cell's regions and other regions are represented by black arrows.

accommodate any constraint on the optimization parameters $\boldsymbol{x}$ as long as it can be embedded into a rectangular parameter space.[3] In this study, we exploit the following bijection:

$$\underbrace{\left(p_i^{(in)}, p_i^{(out)}\right)}_{\boldsymbol{p}_i} \rightarrow \underbrace{\left(p_i^{(in)} + p_i^{(out)}, \frac{p_i^{(out)}}{p_i^{(in)} + p_i^{(out)}}\right)}_{\boldsymbol{x}_i}.$$

Consequently, we consider that the cellular network parameters to optimize are $\boldsymbol{x} = (\boldsymbol{x}_1, \cdots, \boldsymbol{x}_n) \in \mathcal{D}$ with

$$\mathcal{D} = \mathcal{D}^{(1)} \times \cdots \times \mathcal{D}^{(n)} = \left([P_-, P_+] \times \left[\frac{1}{2}, 1\right)\right)^n. \quad (5)$$

Having defined the parameter space $\mathcal{D}$ for the considered RSMs, we turn to the specification of the objective function f. Given a configuration $\boldsymbol{x}_t$ of the cellular network, we consider the achievable rate $c^{(j)}(\boldsymbol{x}_t)$ of each UE $j \in [1, m]$ at time t, with respect to the propagation model $\mathcal{P}$ (see Section IV-D), as the main performance metric to optimize at the UE scale.[4] Consequently, the performance metrics at the cellular network scale are $\boldsymbol{c}(\boldsymbol{x}_t) = \left(c^{(1)}(\boldsymbol{x}_t), \cdots, c^{(m)}(\boldsymbol{x}_t)\right) \in \mathbb{R}^m$.

To turn these performance metrics into a scalar objective value, we consider the α-fairness, introduced by [51]:

$$F_\alpha(\boldsymbol{c}_t) = \begin{cases} \sum_{j=1}^{m} \log c_t^{(j)} & \text{if } \alpha = 1, \\ \sum_{j=1}^{m} \frac{\left(c_t^{(j)}\right)^{1-\alpha}}{1-\alpha} & \text{otherwise,} \end{cases} \quad (6)$$

where, by a slight abuse of notation, $c_t^{(j)}$ denotes $c^{(j)}(\boldsymbol{x}_t)$.

Observe that (6) leads to natural trade-offs between the sum of the rates in $\boldsymbol{c}_t$ and the fairness of these rates. In fact, α controls the importance of fairness in the objective function. As examples, $\alpha = 0$ defines the sum-rate as the objective function, $\alpha = 1$ boils down to the proportional fairness and, since $\lim_{\alpha \to +\infty} F_\alpha(\boldsymbol{c}_t) = \min_{j \in [1,m]} c_t^{(j)}$, $\alpha \to +\infty$ can be viewed as one of the most stringent definitions of fairness.

[3]Otherwise, a constrained BO algorithm for $\mathcal{B}$ would be required (e.g., see [50]).

[4]Note that other performance metrics, such as Energy Efficiency (EE), could have been used in our framework as objective functions to optimize.

Because of its versatility, we use (6) as the objective function of the cellular network. To derive the final form of the objective function, it is essential to determine how resources should be allocated among the UEs within the same region. To avoid introducing an arbitrary policy that could negatively impact the cellular network's performance, we adopt the optimal Time-Division Multiple Access (TDMA) or scheduling policy for each region k within each cell. Given a set $\mathcal{A}^{(k)}$ of $m^{(k)}$ UEs belonging to a region k, we define the optimal scheduling policy $\boldsymbol{s}^{(k)} = \left(s_j^{(k)}\right)_{j \in \mathcal{A}^{(k)}}$ as the solution of

$$\begin{aligned} &\underset{\boldsymbol{s} \in [0,1]^{m^{(k)}}}{\text{maximize}} \; F_\alpha\left(\boldsymbol{s} \odot \boldsymbol{c}_t^{(k)}\right) \\ &\text{s.t.} \qquad \boldsymbol{s}^\top \mathbf{1} = 1 \end{aligned} \quad (7)$$

with $\boldsymbol{c}_t^{(k)} = \left(c_t^{(j)}\right)_{j \in \mathcal{A}^{(k)}}$, $\mathbf{1}$ a conformable vector of ones and $\odot$ the Hadamard product.

$\boldsymbol{s}^{(k)}$ is a vector of size $m^{(k)}$ that sums up to one. Intuitively, its ith element is the fraction of time allocated to the ith UE for transmission.

Proposition 1: The optimal scheduling policy for a set $\mathcal{A}^{(k)}$ of UEs is $\boldsymbol{s}^{(k)} = \left(s_j^{(k)}\right)_{j \in \mathcal{A}^{(k)}}$, with

$$s_j^{(k)} = \begin{cases} \mathbf{1}_{j=j^*} & \text{if } \alpha = 0, \\ \frac{\left(c_t^{(j)}\right)^{(1-\alpha)/\alpha}}{\sum_{i \in \mathcal{A}^{(k)}} \left(c_t^{(i)}\right)^{(1-\alpha)/\alpha}} & \text{otherwise,} \end{cases} \quad (8)$$

with $j^* = \arg\max_{j \in \mathcal{A}^{(k)}} c_t^{(j)}$ and $\mathbf{1}_{j=j^*}$ the indicator function indicating if j is the index of the UE that has the largest rate among the UEs in $\mathcal{A}^{(k)}$.

Proof (Sketch): The special case $\alpha = 0$ is trivial to solve as the solution to maximize the sum-rate is to find the UE that has the largest rate and let it use the full resource.

For $\alpha \neq 0$, the function in the constrained problem (7) is concave with respect to $\boldsymbol{s}$ since it is a sum of concave functions (see (6)). Therefore, it can be turned into an unconstrained problem by considering its Lagrangian relaxation $\mathcal{L}_\alpha(\boldsymbol{s}, \lambda)$,

and its solution is one of the critical points of $\mathcal{L}_\alpha$, found by the criterion $\nabla\mathcal{L}_\alpha = 0$. The relaxation for $\alpha \neq 1$ is

$$\begin{aligned}\mathcal{L}_\alpha(\boldsymbol{s},\lambda) &= F_\alpha\left(\boldsymbol{s}\odot\boldsymbol{c}_t^{(k)}\right) - \lambda\left(\boldsymbol{s}^\top\mathbf{1}-1\right)\\ &= \frac{1}{1-\alpha}\sum_{j\in\mathcal{A}^{(k)}}^{k} s_j^{1-\alpha}\left(c_t^{(j)}\right)^{1-\alpha}\\ &\quad -\lambda\left(\sum_{j\in\mathcal{A}^{(k)}} s_j - 1\right). \end{aligned} \tag{9}$$

Computing the gradient $\nabla\mathcal{L}_\alpha$ by differentiating (9) is trivial, as is solving the system of equations $\nabla\mathcal{L}_\alpha = 0$ for $\boldsymbol{s}$. It yields a single critical point, which is the solution of (7) given in (8). Applying the same technique to the special case $\alpha = 1$ yields the same solution.

We can now derive the form of the objective function. Let $\mathcal{A} = \left\{\mathcal{A}^{(1)},\cdots,\mathcal{A}^{(r)}\right\}$ be the set of all regions in the cellular network,[5] the objective function is

$$f_\alpha(\boldsymbol{x}_t) = \sum_{\mathcal{A}^{(k)}\in\mathcal{A}}\sum_{j\in\mathcal{A}^{(k)}} F_\alpha\left(\boldsymbol{s}^{(k)}\odot\boldsymbol{c}^{(j)}(\boldsymbol{x}_t)\right) \tag{10}$$

with F_α and $\boldsymbol{s}^{(k)}$ given by (6) and (8), respectively.

C. BO Algorithm $\mathcal{B}$

In the context of our study, the optimization problem (1) may have up to $2n$ parameters for a cellular network comprising n BSs (see Section IV-B). In the BO literature, this problem is considered high-dimensional even for medium-sized networks (say $n > 7$). Furthermore, we would like to address the problem (1) in a decentralized fashion, as it would ease the replication of this study in a real cellular network.

To do so, we rely on INSPIRE, the decentralized, high-dimensional BO algorithm proposed in [37]. INSPIRE is initially designed to optimize a $2n$-dimensional proportional fairness within a wireless local-area network (WLAN) comprising n nodes. The problem is addressed in a decentralized fashion, under the assumption that the interference experienced by a UE j associated with a node i is caused solely by a subset of nodes, defined as a neighborhood of node i and denoted $\mathcal{N}_i$.

Note that the proportional fairness optimized by INSPIRE is a special case ($\alpha = 1$) of the objective function (10). Moreover, because (10) is based on the achievable rates of the UEs (and hence, on their SINRs), considering that only the neighborhood of BS i causes the interference of its associated UEs is a mild assumption. Therefore, INSPIRE is a good candidate for the black-box optimization of (10).

Assumption 1:

$$f_\alpha(\boldsymbol{x}_t) \approx \sum_{i=1}^{n}\sum_{\mathcal{A}^{(k)}\in\mathcal{A}_i}\sum_{j\in\mathcal{A}^{(k)}} F_\alpha(\boldsymbol{s}^{(k)}\odot\boldsymbol{c}^{(k)}(\boldsymbol{x}_t^{(\mathcal{N}_i)})) \tag{11}$$

with $\mathcal{A}_i$ the regions controlled by BS i, $\boldsymbol{x}_t^{(\mathcal{N}_i)} = \left(\boldsymbol{x}_t^{(i')}\right)_{i'\in\mathcal{N}_i}$ and $\mathcal{N}_i$ comprising all the BSs at radio range of BS i (including BS i itself).

[5]Note that $r = n$ or $r = 2n$ depending on the considered RSM.

To apply INSPIRE, we need an additive decomposition of the objective function. Let us denote by $|\mathcal{N}_i|$ the cardinality of $\mathcal{N}_i$ and consider $f_\alpha^{(i)} : \mathcal{D}^{(\mathcal{N}_i)} \to \mathcal{D}$, with $\mathcal{D}^{(\mathcal{N}_i)} = \prod_{i'\in\mathcal{N}_i}\mathcal{D}^{(i')}$, such that

$$f_\alpha^{(i)}\left(\boldsymbol{x}_t^{(\mathcal{N}_i)}\right) = \sum_{i'\in\mathcal{N}_i}\sum_{\mathcal{A}^{(k)}\in\mathcal{A}_{i'}}\sum_{j\in\mathcal{A}^{(k)}}\frac{F_\alpha(\boldsymbol{s}^{(k)}\odot\boldsymbol{c}^{(k)}(\boldsymbol{x}_t^{(\mathcal{N}_{i'})}))}{|\mathcal{N}_{i'}|}. \tag{12}$$

Observe that $f_\alpha^{(i)}$ is an additive decomposition of (11). That is, it is trivial to show that

$$f_\alpha(\boldsymbol{x}_t) = \sum_{i=1}^{n} f_\alpha^{(i)}\left(\boldsymbol{x}_t^{(\mathcal{N}_i)}\right). \tag{13}$$

We can now introduce the standard assumptions used in decentralized BO, starting with the Lipschitz continuity.

Assumption 2: $\forall i \in [1,n]$, $f_\alpha^{(i)}$ is Lipschitz continuous with Lipschitz constant $L^{(i)}$, that is

$$\forall\boldsymbol{x},\boldsymbol{x}'\in\mathcal{D}^{(\mathcal{N}_i)}, |f_\alpha^{(i)}(\boldsymbol{x}) - f_\alpha^{(i)}(\boldsymbol{x}')| \leq L^{(i)}||\boldsymbol{x}-\boldsymbol{x}'||_2 \tag{14}$$

Intuitively, Assumption 2 implies that the rate of change of (12) is bounded by $L^{(i)}$ across its entire domain. Finally, we introduce GPs as surrogate models for f_α.

Assumption 3: $\forall i \in [1,n]$, $f_\alpha^{(i)}$ described with (12) is a Gaussian process $\mathcal{GP}^{(i)}\left(0, k^{(i)}\left(\boldsymbol{x},\boldsymbol{x}'\right)\right)$, with $\boldsymbol{x},\boldsymbol{x}' \in \mathcal{D}^{(\mathcal{N}_i)}$.

With Assumption 3, each GP $\mathcal{GP}^{(i)}$ is a surrogate model for the corresponding term $f_\alpha^{(i)}$. Assumption 3 naturally implies that the objective function f itself is a GP, since a linear combination of GPs is also a GP.

Under Assumptions 1, 2 and 3, INSPIRE (as described in [37]) can be run in a decentralized fashion at every BS. Note that, under these assumptions, INSPIRE finds the global maximum of a tight lower bound of the objective function f. Since INSPIRE is a BO algorithm, its computational complexity is in $\mathcal{O}(t^3)$, where t is the number of observations.

D. Propagation Model $\mathcal{P}$

1) Single Antenna: The radio spectrum bandwidth W is shared among all BSs (accordingly to the RSM $\mathcal{R}$) while, locally, each BS shares its spectrum divided into resource blocks (RBs) among all its associated UEs. The average radio link gain between one BS i and one UE j is given by:

$$g_{i,j} = g_0 \cdot s_{i,j} \cdot d_{i,j}^{-\alpha}, \tag{15}$$

where g_0 and α are the standard parameters of a distance-based propagation model, $s_{i,j}$ stands for shadowing and $d_{i,j}$ is the distance between the BS i and the UE j. It is worth mentioning that this channel gain is an average gain for a given pair (i,j) and does not consider random variations due to fading. The impact of fading is discussed hereafter and in Appendix B, where the effective SINR used in this paper is described and motivated.

For each RSM $\mathcal{R}$, we compute the SINRs using power densities. Although this boils down to the well-known SINR expressions for three of the considered RSMs (namely `FR`,

TABLE I
POWER DENSITIES OF THE INTERFERENCE CAUSED BY AN UE j' (ASSOCIATED WITH A BS I) AND SUFFERED BY AN UE J (ASSOCIATED WITH A BS OF THE SAME COLOR)

Region of UE j	UE j and UE j' on same BS?	Region of UE j'	Interference (dBm/Hz)
Inner	Yes	Inner	0
		Outer	0
	No	Inner	$g_{i,j}p_1^{(i)}/W$
		Outer	$g_{i,j}p_2^{(i)}/W$
Outer	Yes	Inner	$g_{i,j}p_1^{(i)}/W$
		Outer	0
	No	Inner	$g_{i,j}p_1^{(i)}/W$
		Outer	$Kg_{i,j}p_2^{(i)}/W$

COLORING and FFR described in Section IV-A), let us derive the SINR expressions for the two NOMA-based RSMs.

Recall that, in these schemes, each BS has to classify its UEs into two classes: strong UEs and weak UEs (see Appendix A). Strong UEs are typically located around the BS whereas weak UEs tend to be located nearby the cell edge. Thus, the service area of a BS can be divided into two regions: the inner region containing all strong UEs and the outer region containing all weak UEs. Additionally, BS i must handle two transmission power levels: $p_i^{(in)}$ for strong UEs and $p_i^{(out)}$ for weak UEs (see Section IV-B). Finally, observe that NOMA+FR is a special case of NOMA+FFR with a number of colors $K = 1$ (see Figure 1).

Following the SIC strategy, strong UEs first decode the signal for weak UEs and cancel their interference, whereas weak UEs decode only their own signal. Note that the latter do not experience strong interference from inner UEs signals thanks to the chosen parameters domain (5) enforcing $p_i^{(in)} \leq p_i^{(out)}$.

The power density for an inner UE (resp. outer UE) associated with a BS i is simply given by $dp_1^{(i)} = p_1^{(i)}/W$ (resp. $dp_2^{(i)} = Kp_2^{(i)}/W$). Table I indicates the expression of the interference power densities according to the UEs' locations. Observe that, in agreement with Figure 1, an inner UE does not suffer interference resulting from transmissions to outer UEs of the same cell (thanks to SIC). Conversely, an inner UE suffers interference resulting from transmissions to UEs associated to a different BS i (be they in the inner or outer region). In that case, the transmission in the outer region causes an interference of power density $\frac{g_{i,j}p_2^{(i)}}{W/K}$ mW/Hz, but only applied to a fraction W/K of the frequency band. Therefore, when considering the average of the power density over the whole frequency band of size W, it boils down to a power density of $\frac{1}{K}\frac{g_{i,j}p_2^{(i)}}{W/K} = \frac{g_{i,j}p_2^{(i)}}{W}$. Note that a more accurate allocation may be done by letting the BS allocate a RB in the sub-band with the lowest interference to each of its inner UEs. This is kept out of the scope of this paper.

The SINRs resulting from this strategy for an inner UE j and an outer UE j' associated with a BS i, denoted by $\gamma_{i,j}^{(in)}$ and $\gamma_{i,j'}^{(out)}$, respectively, are:

$$\gamma_{i,j}^{(in)} = \frac{g_{i,j}p_1^{(i)}}{W_jN + \sum_{i' \in \mathcal{N}\setminus\{i\}} g_{i',j}(p_1^{(i')} + p_2^{(i')})} \tag{16}$$

$$\gamma_{i,j'}^{(out)} = \frac{Kg_{i,j'}p_2^{(i)}}{W_jN + g_{i,j'}p_1^{(i)} + \sum_{i' \in \mathcal{N}\setminus\{i\}} g_{i',j'}(p_1^{(i')} + \delta_{i,i'}Kp_2^{(i')})}, \tag{17}$$

where N is the noise power density and $\delta_{i,i'}$ is equal to 1 if i and i' use the same color for outer UEs, and 0 otherwise.

The SINRs (16) and (17) correspond to effective SINRs as described in detail in Appendix B. Then, for a given effective SINR, the achievable rate of a UE j associated with a BS i follows the model derived in Appendix B and is given by the modified Shannon capacity [52]:

$$c^{(j)} = c(\gamma_{i,j}) = W_j \cdot \kappa \log_2(1 + \beta\gamma_{i,j}) \tag{18}$$

where W_j is the bandwidth used by the UE j. As the purpose of this study is to illustrate the evaluation framework proposed in Section III under a simple simulation model, we introduce κ and β to encapsulate the performance loss of a real system, due to imperfect modulation, coding schemes, and imperfect radio. Finally, we use $\tilde{\gamma}_{i,j} = \min(\gamma_{i,j}, \gamma_{\max})$ dB to prevent cases where the SINR $\gamma_{i,j}$ computed with (16) and (17) is diverging.

2) Extensions to Multi-Antennas: In the case of multi-antennas equipments (both at the transmitter and the receiver), 4G Long-Term Evolution (LTE) and beyond standards allow to increase the effective SINR and the associated capacity by using a combination of diversity, multiplexing and Multi-User Multiple Input Multiple Output (MU-MIMO). Our model remains valid to study any specific transmission mode as defined in [53]. In this case, (16) and (17) are replaced by

$$\gamma_{i,j}^{(in)} = \frac{c_0 g_{i,j}p_1^{(i)}}{W_jN + c_2 \sum_{i' \in \mathcal{N}\setminus\{i\}} g_{i',j}(p_1^{(i')} + p_2^{(i')})} \tag{19}$$

$$\gamma_{i,j'}^{(out)} = \frac{c_0 Kg_{i,j'}p_2^{(i)}}{W_jN + g_{i,j'}p_1^{(i)} + c_2 \sum_{i' \in \mathcal{N}\setminus\{i\}} g_{i',j'}(p_1^{(i')} + \delta_{i,i'}Kp_2^{(i')})}, \tag{20}$$

where c_0 and c_2 are the constant defined in Appendix B. The constant c_0 (*i.e.*, the receiver gain) is lower than the number of reception antennas, while the interference rejection c_2 is lower than 1 and its exact value depends on the beamforming strategy as well as partial coordination in resource management between BSs.

Furthermore, the simultaneous transmission of multiple flows as proposed in some LTE modes, as described in Appendix B, provides a capacity gain G_m up to the number of layers (or streams). With such multiplexing, (18) becomes

$$c^{(j)} = c(\gamma_{i,j}) = G_m W_j \kappa \log_2(1 + \beta\gamma_{i,j}). \tag{21}$$

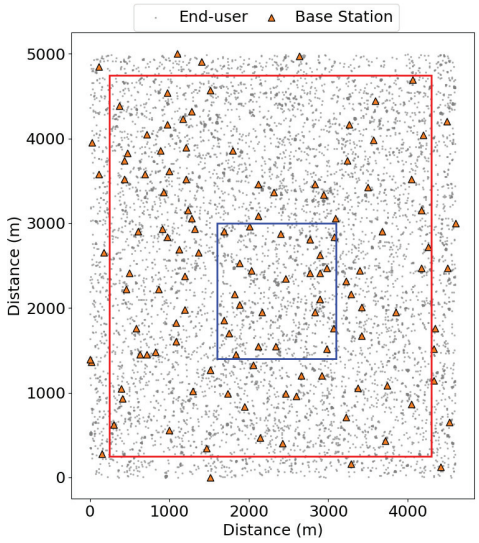

Fig. 2. Illustration of the simulated cellular network, inspired by Orange's cellular deployment in Lyon. The blue rectangle depicts the subset of BSs shown in Figure 6 while the red rectangle depicts the subset of the BSs used to collect our performance metrics (see Figures 3, 4, 5 and Table III).

In this study we consider both beamforming gains and interference rejection, but without multiplexing. In our model, we set $G_m = 1$ (no multiplexing gain), and $c_2 = 1/c_0$ with $G_b(c_0) \in \{0, 3, 6\}$ where $G_b(c_0) = 10\log_{10}(c_0)$ (dB) in the SINR of all UEs (see (19) and (20)).

E. Cellular Network Topology $\mathcal{T}$

Finally, we specify the cellular network topology considered in this study. We simulate the cellular network deployed in the city of Lyon, France by the main French mobile network operator (Orange). The precise locations of the BSs are made publicly available by a French national agency [54].

We consider a Log-Gaussian Cox process to generate a realistic spatial distribution of UEs that contains clusters and empty regions. Let us describe briefly how we implemented the process (for a thorough description, please refer to [55]). The domain containing the cellular network is split into tiles of 25 meters-long sides. For each tile k, a Gaussian random variable $X_k \sim \mathcal{N}(\mu, \sigma^2)$ is sampled. Then Y_k, the number of UEs within the tile k, is sampled from a Poisson distribution of intensity e^{X_k}, that is $Y_k \sim \text{Pois}(e^{X_k})$. Finally, Y_k UEs are uniformly generated within the tile. In our scenario, we set the parameters so that the process generated a set of UEs with a global spatial density similar to the one observed in Lyon ($\approx$ 11,000 persons / km^2). Then, a fraction of these UEs was randomly selected according to the market share of Orange in France ($\approx 38.5\%$). Finally, 10% of the UEs from this subset were randomly selected to account for active UEs only.

Figure 2 illustrates the obtained cellular network, with 125 BSs and around 9,000 UEs. Note that, in the next section, we collect and discuss performance metrics on the BSs (and their associated UEs) located within the red rectangle, to limit artifacts at the border of the simulated network.

TABLE II
HOMEMADE SIMULATOR PARAMETERS

Name	Value
Background noise N	-160 dBm/Hz
Path Loss	$\texttt{LogDistance}(d_{\text{ref}} = 1$ km, $L_{\text{ref}} = 128.1$ dBm, $n = 3.76)$
Bandwidth W	20 MHz
Beamforming gain	Within $[0, 6]$ dB
Shannon capacity coefs.	$\kappa = \beta = 1$
Maximal SINR $\gamma_{\max}$	27 dB
Optimization steps	110
GP covariance function k	Matérn ($\nu = \frac{3}{2}$) [43]
Acquisition function	Expected Improvement [47]

TABLE III
FIRST, SECOND AND THIRD QUARTILES FOR UES' RATES DISTRIBUTIONS (IN MBPS) WHEN $\alpha = 2$

	Beamforming Gain								
	0 dB			3 dB			6 dB		
RSM	Q25	Q50	Q75	Q25	Q50	Q75	Q25	Q50	Q75
FR	0.19	0.30	0.55	0.38	0.65	1.03	0.56	0.87	1.75
COL	0.15	0.22	0.40	0.18	0.29	0.51	0.21	0.36	0.63
FFR	0.18	0.30	0.57	0.29	0.47	0.80	0.40	0.62	1.09
NOMA+FFR	**0.22**	0.33	0.65	0.37	0.68	1.15	0.55	0.99	1.83
NOMA+FR	0.21	**0.34**	**0.68**	**0.49**	**0.81**	**1.45**	**0.83**	**1.61**	**2.37**

V. NUMERICAL RESULTS

In this section, we illustrate the proposed evaluation framework (see Section III) by implementing all its ingredients according to the specifications described in Section IV in our homemade simulator to present insightful data about the performance of NOMA in a multi-cell context. Table II collects the main simulation parameters. Note that most of them are kept as simple as possible to prioritize the interpretability of our results. However, since the objective function is treated as a black box, our performance evaluation framework can be utilized to address "what if" scenarios under different conditions or combined with a more realistic simulator. More specifically, we study the distribution of the UEs' spectral efficiencies, the distribution of their achievable rates (see (18)) and the quality of the capacity-fairness tradeoff made by each RSM at the cellular network scale.

First, let us study the distribution of the UEs' spectral efficiencies. Figure 3 depicts their cumulative distribution functions (CDFs), for each considered RSM, different fairness constraints α (see (6)) and beamforming gains. Although the fairness constraint α has virtually no effect on the CDFs, the benefits of using beamforming are substantial. In fact, the spectral efficiencies directly depend on the UEs' SINRs (see (18)), which get larger when the beamforming gain increases. This is illustrated by the right shift experienced by the CDFs as the beamforming gain increases. Finally, as one could expect, the RSMs exploiting orthogonal resources (COLORING and FFR) are the most spectrally efficient. This can be deduced by observing that the corresponding CDFs are consistently the lowest ones for a given spectral efficiency. Note that this is no guarantee of a larger achievable rate, as these RSMs allocate only fractions of the available bandwidth to each of their UEs.

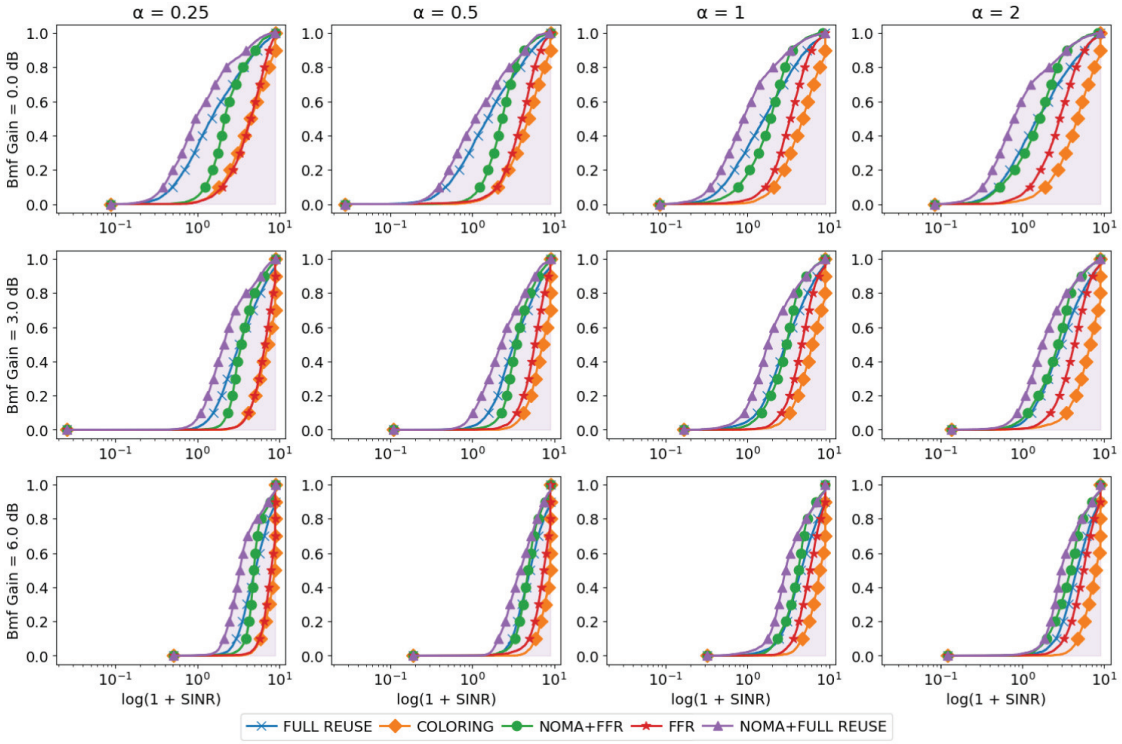

Fig. 3. The cumulative distribution functions of the UEs' spectral efficiencies (expressed as $\log_2(1 + \text{SINR})$) in the simulated cellular network, for each RSM, several fairness constraints α (column-wise) and multiple beamforming gains (row-wise). Note that for each plot, the x-axis is in log-scale.

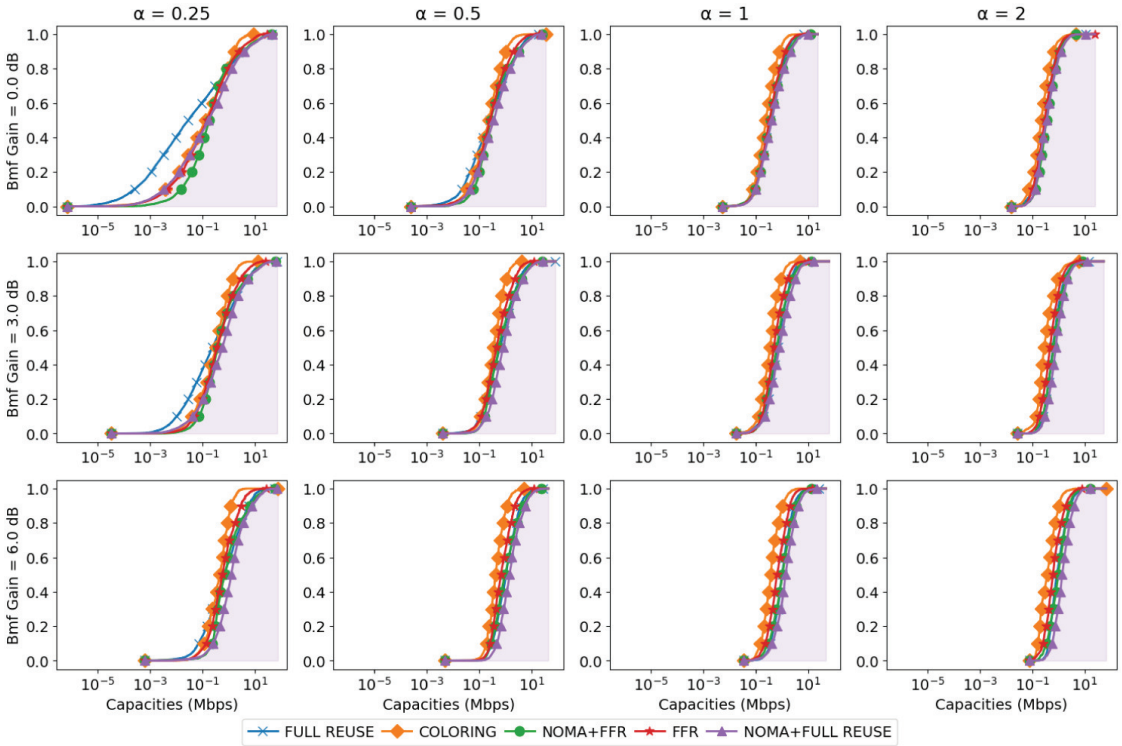

Fig. 4. The cumulative distribution functions of the UEs' Shannon capacities in the simulated cellular network (in Mbps), for each RSM, several fairness constraints α (column-wise) and multiple beamforming gains (row-wise). Note that for each plot, the x-axis is in log-scale.

We now turn to the distribution of the UEs' achievable rates. Figure 4 depicts the CDFs of the UEs' rates, for each considered RSM, different fairness constraints α and beamforming gains. As one could expect, the distribution

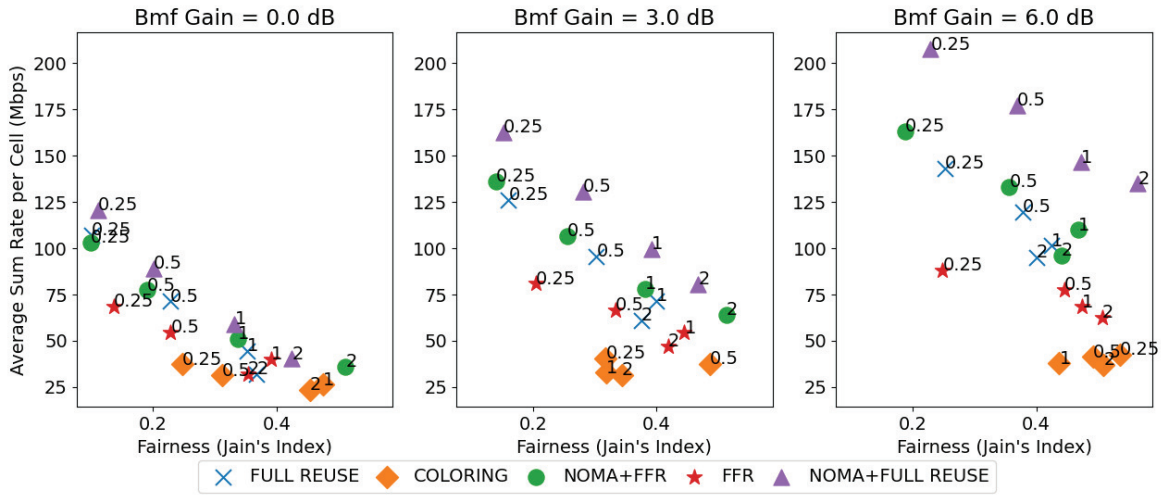

Fig. 5. The performance of each RSM in terms of sum rate and fairness (Jain). Each plot corresponds to a different value of the beamforming gain. By changing the value of α, Pareto fronts appear in the output space and allow the comparison between RSMs.

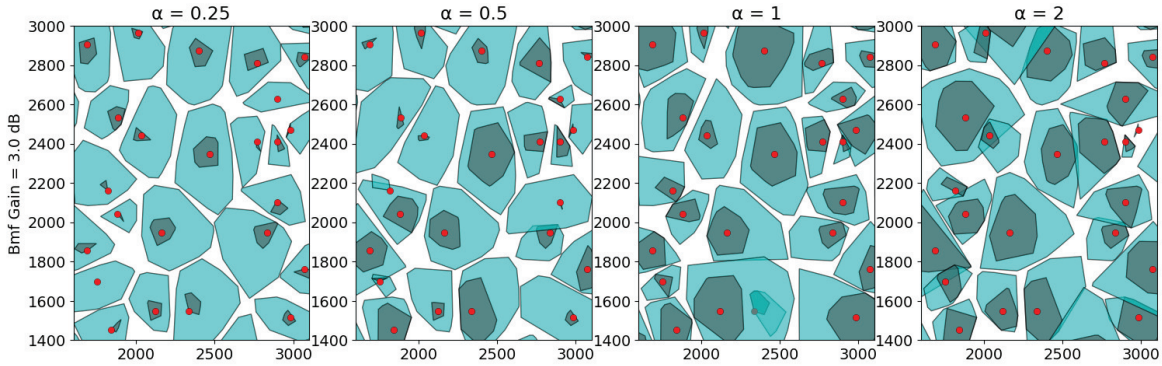

Fig. 6. A subset of the cellular network configured by the best configurations of NOMA+FULL_REUSE, found by INSPIRE for a beamforming gain of 3 dB and several values of α. Each BS is shown with a red dot. Each cell is depicted with the convex hull of its associated UEs. Finally, the shaded areas depict the inner regions of the cells.

of rates among UEs is more spread when the fairness constraint α is low, and more concentrated when α is large. As an example, observe at the top row of Figure 4 that the distributions' supports spread over no less than eight orders of magnitude when $\alpha = 0.25$ (from 10^{-6} to 10^{2} Mbps) while they only cover 3 orders of magnitude when $\alpha = 2$ (from 10^{-1} to 10^{1} Mbps). Additionally, and similarly to the spectral efficiency (see Figure 3), increasing the beamforming gain significantly improves the rates. Finally, observe that the CDF of NOMA+FULL_REUSE is consistently the lowest among all the CDFs. This intuitively translates into the fact that NOMA+FULL_REUSE systematically ensures better (*i.e.*, larger) rates for its UEs.

For a comparison between RSMs that is more quantitative than what Figure 4 allows, we provide Table III. The 25%, 50% and 75% quantiles of the UEs' rates distributions are reported for each considered RSM, beamforming level and a fairness constraint $\alpha = 2$. The best quantile value among all RSMs is written in bold. NOMA+FULL_REUSE consistently appears as the RSM providing the best rate for all beamforming gains and all quantiles reported, sometimes by a considerable margin.

To further study the rate-fairness tradeoffs achieved by the RSMs, we consider a 2-dimensional space, called the *output space*, with the average sum rate per cell and the fairness (according to Jain's index [56]) as dimensions. By varying α, one can compare how the achieved tradeoffs evolve when the incentive for a fair distribution of the rates changes. These trajectories draw Pareto fronts in the output space, and Pareto-dominance [57] can be used to rank the RSMs. Figure 5 depicts the performance of the RSMs in the output space, for several beamforming gains. Observe that the NOMA-based RSMs appear to find better tradeoffs than FFR and COLORING across all the considered values of α and all beamforming gains. They also appear equivalent to FULL REUSE when no beamforming gain is considered (except for $\alpha = 2$ where they manage to get better rates and fairness than all the other RSMs). With positive beamforming gains, NOMA+FULL_REUSE Pareto-dominates all the other RSMs (including NOMA+FFR), for almost all the considered values

of α. In accordance to the CDFs observed in Figure 4 and to the values reported in Table III, FFR and COLORING obtain significantly lower performance metrics, while FULL REUSE gets slightly lower performance metrics than NOMA+FFR.

Finally, Figure 6 shows a subset of the cellular network corresponding to the blue rectangle in Figure 2, for the NOMA+FULL_REUSE mechanism. The impact of the fairness constraint α on the cells' geometry can be easily visualized: the larger the value of α, the bigger the inner regions of the cells. Note that, because the cells are depicted with the convex hulls of their associated UEs, some cells may overlap in the visualization.

Overall, our results suggest that NOMA combined with a full-reuse policy (denoted NOMA+FULL_REUSE in our experiments) consistently emerges as the RSM that finds the best tradeoff between a large sum of rates and a large fairness. This may be an important piece of information when designing the next-generation of cellular networks.

VI. Conclusion

In this paper, we proposed a general framework to fairly evaluate an arbitrary RSM in a complex, multi-cell context. Such evaluations cannot be handled by classical tools based on stochastic geometry, or on algorithmic designs, due to unrealistic knowledge requirements or prohibitive computational costs. Unlike these, our framework allows the evaluation of an arbitrary RSM by solving a difficult optimization problem under a minimal set of assumptions. To address this challenge, we leveraged recent advances in the black-box optimization literature by exploiting a distributed BO algorithm. The use of a BO algorithm ensures the desired versatility of our framework (*i.e.*, no specific assumptions about the cellular network or the interference model in use). In fact, the proposed evaluation framework could be paired to any simulator or implemented on a real-life network.

Using this evaluation framework, we compared five RSMs: full reuse, graph coloring, FFR, a combination of NOMA with FFR and a combination of NOMA with full reuse, under several levels of fairness (*i.e.*, several values of α) and multiple beamforming gains on a real-life inspired scenario for the locations of BSs and UEs. Our results showed that the combination of NOMA with a full reuse policy is able to consistently find better tradeoffs (with respect to sum rate and fairness) than the other RSMs, sometimes by a comfortable margin. We believe that the proposed framework can be of interest to mobile network operators (MNOs) for comparing the efficiency of RSMs on their cellular network deployments. In particular, it is up to MNOs to decide whether the gains brought by NOMA are substantial in light of its additional, though limited, complexity in the case of a 2-user NOMA.

In future work, we plan to replicate the study conducted in Sections IV and V using Monte-Carlo simulations instead of a homemade simulator to provide more complete and realistic insights on the performance of NOMA at the system level. Also, we plan to extend our framework to handle dynamic scenarios where UEs are moving and subject to birth-and-death processes. The BO algorithm in use (denoted $\mathcal{B}$ in the previous sections) would need to be refined, in particular, to manage the potential staleness of previously collected data (e.g., by applying techniques described in [58] and [59]). Compared to state-of-the-art algorithms, such an approach would allow the cells to breathe as a function of their local traffic load (an idea that was used for 3G networks), adapting over time the UEs/BSs association. This is an important feature to contribute to cell-free solutions with limited complexity, as currently investigated for 6G networks.

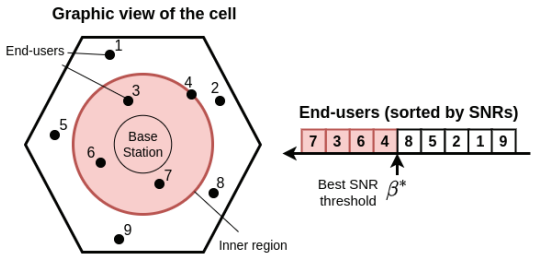

Fig. 7. An illustration of how a cell is split into two regions based on the SNRs of its associated UEs. The cell is shown as an hexagon, the inner region as a red circle and the outer region as the complementary of the circle in the hexagon. The BS is at the center of the cell, and each UE is shown as a black dot.

Acknowledgment

The authors would like to thank the anonymous referees for their thorough and constructive review of an earlier version of this article.

Appendix A
Splitting a Cell Into Two Regions

In this appendix, we describe how we compute the set of all regions $\mathcal{A}$, that is, how the UEs are associated with their BSs and distributed over the two regions of each cell.

First, recall that given a configuration $\boldsymbol{x}_t \in \mathcal{D}$, each UE associates with the BS that provides the best SINR.

Then, within each cell *i*, the optimal 2-partition of the set of associated UEs (*i.e.*, the one that maximizes (10) within the cell) must be computed. Note that since each UE *j* knows its SINR with its BS, its achievable rate $c^{(j)}$ and, a fortiori, the objective function (10) within the cell can be computed. Because there exist $2^{m^{(i)}-1}-1$ partitions if the cell *i* contains $m^{(i)}$ UEs, using a greedy algorithm that explores all the partitions would be prohibitive.

To circumvent this combinatorial problem, all the associated UEs are sorted by SNR in descending order. Then, the set of UEs is partitioned based on a SNR threshold β: the UEs with a SNR larger than β are associated with the inner region, while the others are associated with the outer region. The objective function (10) is computed for all the $m^{(i)}-1$ 2-partitions of the list of ordered SNRs in order to determine β^*, which is the SNR threshold associated with the 2-partition that yields the largest value of (10). Figure 7 illustrates how β^* is computed.

Appendix B
UEs' Effective SINRs and Rates

4G and beyond networks use OFDMA to share the resources with multiple UEs. The spectrum is divided in several Physical

Resource Blocks (PRB) and each UE gets a subset of PRBs. In most real environment the channel gain associated to each PRB is entailed by variations due to fading. Thus the channel gain between each Tx-Rx pair g_{ij} is subject to random variations which impacts the SINR and the associated rates. In the context of LTE, as described in [60], a transmission over multiple PRBs is performed across many channel states. Under standard assumptions on the joint stationarity and ergodicity of the channel coefficients and under perfect channel state information at the receiver (CSIR), the achievable rate of an UE is commonly characterized as the ergodic achievable rate [61]. For a given UE, in a given scenario (active BSs are fixed), the ergodic capacity characterizing an achievable rate is upper bounded, treating interference as noise [62], with

$$R_{ij} \leq \mathcal{C}(\mathbb{E}\left[\gamma_{ij}\right]) = \log_2\left(1 + \frac{G_{ij} dp^{(i)}}{N + \sum_{i' \in \mathcal{N}\setminus\{i\}} G_{i'j} dp^{(i')}}\right). \tag{22}$$

where $G_{ij} = \mathbb{E}[g_{ij}]$ and $dp^{(i)}$ is the power spectral density. The other notations are consistent with the rest of the paper.

This bound is not always achievable and in [61], following [63], and exploiting Jensen inequality, the multi-RB ergodic rate is lower bounded by:

$$R_{ij} \geq \log_2\left(1 + \frac{\mathbb{E}\left[\zeta_{ij}\right]^2}{N + \text{var}[\zeta_{ij}] + \sum_{i' \in \mathcal{N}\setminus\{i\}} \mathbb{E}\left[|\zeta^c_{i'j}|^2\right]}\right), \tag{23}$$

where ζ_{ij} are the amplitude of the random received signal, according to the notations detailed in [61].

Based on this analysis, we define an effective SINR, that can be made close to the upper bound:

$$\gamma_{i,j} = \frac{c_0 g_{i,j} p_1^{(i)}}{WN + c_1 g_{i,j} p^{(i)}) + c_2 \sum_{i' \in \mathcal{N}\setminus\{i\}} g_{i',j} p^{(i')})} \tag{24}$$

where c_0, c_1 and c_2 are tuning parameters representing the receiver gain ($c_0 \geq R_a$, where R_a is the number of received antennas), the maximal SINR leakage due to self-interference ($c_1 \leq 1$) and the interference rejection gain ($c_2 < 1$).

Equations (16) and (17) in Section IV-D.1 are directly derived from this effective SINR expression, using $p^{(i)} = W \cdot dp^{(i)}$ and $(c_0, c_1, c_2) = (1, 0, 1)$ for the sake of simplicity.

This effective SINR model can be extended to MIMO scenarios according to the modes used in 4G and 5G standards. Taking Release 13 of the 3GPP as a reference [53], several transmission modes are defined for the Physical Downlink Shared Channel (PDSCH). We describe a few of them below:

- Mode 1 is single antenna; in this case, the former model holds. Diversity may be used at the receiver. Usually, the receiver has between 2 to 4 active antennas.
- Modes 2, 3 and 4 use diversity with precoding. Consequently, c_1 can be reduced in (24).
- Mode 4 also proposes closed-loop spatial multiplexing. in this mode the multiple antennas are used to transmit multiple data flows simultaneously to the same UE. Appropriate signaling may help to select the precoders to maximise the SINR of the multiple flows. While in 4G it was possible to multiplex up to 2 stream, 5G offers the opportunity to multiplex up to 8 data streams
- Mode 5 is MU-MIMO and allows to transmit simultaneously to multiple UEs.

While the modes based on diversity are compatible with our model, both closed-loop multiplexing and MU-MIMO introduce an additional gain. Indeed, the transmitter optimizes the beam selection to maximize the SINR (fading reduction), but also to multiplex simultaneous transmissions, allowing to increase the overall capacity. The former SINR formulation remains correct with better coefficients c_0, c_1 and c_2 but it also allows to increase the capacity given in (18) with a multiplexing factor (up to 8 in 5G), as given in (21).

REFERENCES

[1] Z. Xu, G. Y. Li, C. Yang, and X. Zhu, "Throughput and optimal threshold for FFR schemes in OFDMA cellular networks," *IEEE Trans. Wireless Commun.*, vol. 11, no. 8, pp. 2776–2785, Aug. 2012.

[2] M. Elwekeil, M. Alghoniemy, O. Muta, A. B. Abdel-Rahman, H. Gacanin, and H. Furukawa, "Performance evaluation of an adaptive self-organizing frequency reuse approach for OFDMA downlink," *Wireless Netw.*, vol. 25, no. 2, pp. 507–519, Feb. 2019.

[3] S. Ezhilarasi and P. T. V. Bhuvaneswari, "Maximization of sum throughput in LTE heterogeneous network using region splitting-based resource partitioning scheme," *Wireless Pers. Commun.*, vol. 121, no. 1, pp. 905–938, Nov. 2021.

[4] W. Shin, M. Vaezi, B. Lee, D. J. Love, J. Lee, and H. V. Poor, "Non-orthogonal multiple access in multi-cell networks: Theory, performance, and practical challenges," *IEEE Commun. Mag.*, vol. 55, no. 10, pp. 176–183, Oct. 2017.

[5] R. Ç. Kızılırmak, "Non-orthogonal multiple access (NOMA) for 5G networks," in *Towards 5G Wireless Networks-A Physical Layer Perspective*, vol. 83. Rijeka, Croatia: InTech, Dec. 2016, pp. 83–98.

[6] Z. Ding, X. Lei, G. K. Karagiannidis, R. Schober, J. Yuan, and V. K. Bhargava, "A survey on non-orthogonal multiple access for 5G networks: Research challenges and future trends," *IEEE J. Sel. Areas Commun.*, vol. 35, no. 10, pp. 2181–2195, Oct. 2017.

[7] M. Vaezi, Z. Ding, and H. V. Poor, *Multiple Access Techniques for 5G Wireless Networks and Beyond*, vol. 159. Cham, Switzerland: Springer, 2019.

[8] S. Sen, N. Santhapuri, R. R. Choudhury, and S. Nelakuditi, "Successive interference cancellation: A back-of-the-envelope perspective," in *Proc. 9th ACM SIGCOMM Workshop Hot Topics Netw.*, 2010, pp. 1–6.

[9] J.-M. Gorce, P. Mary, D. Anade, and J.-M. Kélif, "Fundamental limits of non-orthogonal multiple access (NOMA) for the massive Gaussian broadcast channel in finite block-length," *Sensors*, vol. 21, no. 3, p. 715, Jan. 2021.

[10] M. Vaezi, R. Schober, Z. Ding, and H. V. Poor, "Non-orthogonal multiple access: Common myths and critical questions," *IEEE Wireless Commun.*, vol. 26, no. 5, pp. 174–180, Oct. 2019.

[11] K. Wang, Y. Liu, Z. Ding, A. Nallanathan, and M. Peng, "User association and power allocation for multi-cell non-orthogonal multiple access networks," *IEEE Trans. Wireless Commun.*, vol. 18, no. 11, pp. 5284–5298, Nov. 2019.

[12] S. Elhoushy, M. Ibrahim, and W. Hamouda, "Cell-free massive MIMO: A survey," *IEEE Commun. Surveys Tuts.*, vol. 24, no. 1, pp. 492–523, 1st Quart., 2022.

[13] Y. Liu et al., "Evolution of NOMA toward next generation multiple access (NGMA) for 6G," *IEEE J. Sel. Areas Commun.*, vol. 40, no. 4, pp. 1037–1071, Apr. 2022.

[14] Y.-F. Liu et al., "A survey of recent advances in optimization methods for wireless communications," *IEEE J. Sel. Areas Commun.*, vol. 42, no. 11, pp. 2992–3031, Nov. 2024.

[15] V. Ghanbarzadeh, M. Zahabi, H. Amiriara, F. Jafari, and G. Kaddoum, "Resource allocation in NOMA networks: Convex optimization and stacking ensemble machine learning," *IEEE Open J. Commun. Soc.*, vol. 5, pp. 5276–5288, 2024.

[16] Z. Yang, C. Pan, W. Xu, Y. Pan, M. Chen, and M. Elkashlan, "Power control for multi-cell networks with non-orthogonal multiple access," *IEEE Trans. Wireless Commun.*, vol. 17, no. 2, pp. 927–942, Feb. 2018.

[17] L. Salaun, M. Coupechoux, and C. S. Chen, "Weighted sum-rate maximization in multi-carrier NOMA with cellular power constraint," in *Proc. IEEE Conf. Comput. Commun.*, Apr. 2019, pp. 451–459.

[18] L. Salaun, M. Coupechoux, and C. S. Chen, "Joint subcarrier and power allocation in NOMA: Optimal and approximate algorithms," *IEEE Trans. Signal Process.*, vol. 68, pp. 2215–2230, 2020.

[19] S. Banerjee, C. S. Chen, M. Coupechoux, and A. Sinha, "Joint power and subcarrier allocation in multi-cell multi-carrier NOMA," in *Proc. 13th Int. Conf. Ubiquitous Future Netw. (ICUFN)*, Jul. 2022, pp. 180–185.

[20] S. Rezvani, E. A. Jorswieck, N. M. Yamchi, and M. R. Javan, "Optimal SIC ordering and power allocation in downlink multi-cell NOMA systems," *IEEE Trans. Wireless Commun.*, vol. 21, no. 6, pp. 3553–3569, Jun. 2022.

[21] S. Rezvani, E. A. Jorswieck, R. Joda, and H. Yanikomeroglu, "Optimal power allocation in downlink multicarrier NOMA systems: Theory and fast algorithms," *IEEE J. Sel. Areas Commun.*, vol. 40, no. 4, pp. 1162–1189, Apr. 2022.

[22] C. G. Kang, A. T. Abebe, and J. Choi, "NOMA-based grant-free massive access for latency-critical Internet of Things: A scalable and reliable framework," *IEEE Internet Things Mag.*, vol. 6, no. 3, pp. 12–18, Sep. 2023.

[23] P. Lai et al., "Online user and power allocation in dynamic NOMA-based mobile edge computing," *IEEE Trans. Mobile Comput.*, vol. 22, no. 11, pp. 6676–6689, Nov. 2023.

[24] X. Yu, X. Zhang, Y. Rui, K. Wang, X. Dang, and M. Guizani, "Joint resource allocations for energy consumption optimization in HAPS-aided MEC-NOMA systems," *IEEE J. Sel. Areas Commun.*, vol. 42, no. 12, pp. 3632–3646, Dec. 2024.

[25] D. Kim, H. Jung, I.-H. Lee, and D. Niyato, "Novel resource allocation algorithm for IoT networks with multicarrier NOMA," *IEEE Internet Things J.*, vol. 11, no. 18, pp. 30354–30367, Sep. 2024.

[26] J. G. Andrews, F. Baccelli, and R. K. Ganti, "A tractable approach to coverage and rate in cellular networks," *IEEE Trans. Commun.*, vol. 59, no. 11, pp. 3122–3134, Nov. 2011.

[27] C. Altay and M. Koca, "Fractional frequency reuse in non-orthogonal multiple access heterogeneous networks," in *Proc. IEEE Int. Conf. Commun. (ICC)*, May 2018, pp. 1–6.

[28] J. García-Morales, G. Femenias, and F. Riera-Palou, "Analysis and optimization of FFR-aided OFDMA-based heterogeneous cellular networks," *IEEE Access*, vol. 4, pp. 5111–5127, 2016.

[29] J. García-Morales, G. Femenias, and F. Riera-Palou, "On the design of OFDMA-based FFR-aided irregular cellular networks with shadowing," *IEEE Access*, vol. 6, pp. 7641–7653, 2018.

[30] M. Salehi, H. Tabassum, and E. Hossain, "Meta distribution of SIR in large-scale uplink and downlink NOMA networks," *IEEE Trans. Commun.*, vol. 67, no. 4, pp. 3009–3025, Apr. 2019.

[31] L. Chetot, J.-M. Gorce, and J.-M. Kélif, "Fundamental limits in cellular networks with point process partial area statistics," in *Proc. Int. Symp. Model. Optim. Mobile, Ad Hoc, Wireless Netw. (WiOPT)*, Jun. 2019, pp. 1–8.

[32] Y. Sun, Z. Ding, X. Dai, and O. A. Dobre, "On the performance of network NOMA in uplink CoMP systems: A stochastic geometry approach," *IEEE Trans. Commun.*, vol. 67, no. 7, pp. 5084–5098, Jul. 2019.

[33] S. Kusaladharma, W. Zhu, W. Ajib, and G. Amarasuriya, "Achievable rate analysis of NOMA in cell-free massive MIMO: A stochastic geometry approach," in *Proc. IEEE Int. Conf. Commun. (ICC)*, May 2019, pp. 1–6.

[34] C. Zhang, Y. Liu, and Z. Ding, "Semi-Grant-Free NOMA: A stochastic geometry model," *IEEE Trans. Wireless Commun.*, vol. 21, no. 2, pp. 1197–1213, Feb. 2022.

[35] D. P. Kingma and J. Ba, "Adam: A method for stochastic optimization," 2014, *arXiv:1412.6980*.

[36] Y.-A. Ma, T. Chen, and E. B. Fox, "A complete recipe for stochastic gradient MCMC," in *Proc. Adv. Neural Inf. Process. Syst.*, vol. 28, 2015, pp. 2917–2925.

[37] A. Bardou and T. Begin, "INSPIRE: Distributed Bayesian optimization for ImproviNg SPatIal REuse in dense WLANs," in *Proc. Int. Conf. Model. Anal. Simul. Wireless Mobile Syst. Int. Conf. Model. Anal. Simul. Wireless Mobile Syst.*, Oct. 2022, pp. 133–142.

[38] J. Bergstra, D. Yamins, and D. Cox, "Making a science of model search: Hyperparameter optimization in hundreds of dimensions for vision architectures," in *Proc. 30th Int. Conf. Mach. Learn.*, vol. 28, Feb. 2013, pp. 115–123.

[39] D. Lizotte, T. Wang, M. Bowling, and D. Schuurmans, "Automatic gait optimization with Gaussian process regression," in *Proc. 20th Int. Joint Conf. Artif. Intell.* San Mateo, CA, USA: Morgan Kaufmann, 2007, pp. 944–949.

[40] C. K. I. Williams and C. E. Rasmussen, "Gaussian processes for regression," in *Proc. Conf. Neural Inf. Process. Syst. (NeurIPS)*, 1995, pp. 633–638.

[41] C. A. Micchelli, Y. Xu, and H. Zhang, "Universal kernels," *J. Mach. Learn. Res.*, vol. 7, pp. 2651–2667, 2006.

[42] J. L. Doob, "The Brownian movement and stochastic equations," *Ann. Math.*, vol. 43, no. 2, pp. 351–369, Apr. 1942.

[43] M. G. Genton, "Classes of kernels for machine learning: A statistics perspective," *J. Mach. Learn. Res.*, vol. 2, no. 2, pp. 299–312, Dec. 2002.

[44] N. Srinivas, A. Krause, S. M. Kakade, and M. W. Seeger, "Information-theoretic regret bounds for Gaussian process optimization in the bandit setting," *IEEE Trans. Inf. Theory*, vol. 58, no. 5, pp. 3250–3265, May 2012.

[45] S. S. Gupta and K. J. Miescke, "Bayesian look ahead one-stage sampling allocations for selection of the best population," *J. Stat. Planning Inference*, vol. 54, no. 2, pp. 229–244, Sep. 1996.

[46] D. R. Jones, M. Schonlau, and W. J. Welch, "Efficient global optimization of expensive black-box functions," *J. Global Optim.*, vol. 13, no. 4, pp. 455–492, Dec. 1998.

[47] J. Mockus, "Application of Bayesian approach to numerical methods of global and stochastic optimization," *J. Global Optim.*, vol. 4, no. 4, pp. 347–365, Jun. 1994.

[48] A. Bardou, P. Thiran, and T. Begin, "Relaxing the additivity constraints in decentralized no-regret high-dimensional Bayesian optimization," in *Proc. 12th Int. Conf. Learn. Representations*, 2023, pp. 1–17.

[49] T. T. Joy, S. Rana, S. Gupta, and S. Venkatesh, "Batch Bayesian optimization using multi-scale search," *Knowl.-Based Syst.*, vol. 187, Jan. 2020, Art. no. 104818.

[50] D. Eriksson and M. Poloczek, "Scalable constrained Bayesian optimization," in *Proc. 24th Int. Conf. Artif. Intell. Stat. (AISTATS)*, 2021, pp. 730–738.

[51] J. Mo and J. Walrand, "Fair end-to-end window-based congestion control," *IEEE/ACM Trans. Netw.*, vol. 8, no. 5, pp. 556–567, Oct. 2000.

[52] J. H. B. Kemperman, "On the Shannon capacity of an arbitrary channel," *Indagationes Mathematicae (Proc.)*, vol. 77, no. 2, pp. 101–115, 1974.

[53] *LTE: Evolved Universal Terrestrial Radio Access (E-UTRA); Physical Layer Procedures*, document TS 36.213, 3GPP, 2020.

[54] (2022). *Autorité De Régulation Des Communications Électroniques Des Postes Et De La Distribution De La Presse (ARCEP)*. Accessed: Jul. 27, 2023. [Online]. Available: https://files.data.gouv.fr/arcepdonnees/mobile/sites/2022T3/

[55] J. Møller, A. R. Syversveen, and R. P. Waagepetersen, "Log Gaussian cox processes," *Scandin. J. Statist.*, vol. 25, no. 3, pp. 451–482, Sep. 1998.

[56] R. K. Jain, D.-M. W. Chiu, and W. R. Hawe, "A quantitative measure of fairness and discrimination," Dept. Eastern Res. Lab., Digit. Equip. Corp., Hudson, MA, USA, Tech. Rep. 1, 1984, vol. 21.

[57] M. Voorneveld, "Characterization of Pareto dominance," *Operations Res. Lett.*, vol. 31, no. 1, pp. 7–11, Jan. 2003.

[58] A. Bardou, P. Thiran, and G. Ranieri, "This too shall pass: Removing stale observations in dynamic Bayesian optimization," in *Proc. Adv. Neural Inf. Process. Syst.*, 2024, pp. 1–36.

[59] A. Bardou and P. Thiran, "Optimizing through change: Bounds and recommendations for time-varying Bayesian optimization algorithms," 2025, *arXiv:2501.18963*.

[60] E. Biglieri, J. Proakis, and S. Shamai (Shitz), "Fading channels: Information-theoretic and communications aspects," *IEEE Trans. Inf. Theory*, vol. 44, no. 6, pp. 2619–2692, Oct. 1998.

[61] G. Caire, "On the ergodic rate lower bounds with applications to massive MIMO," *IEEE Trans. Wireless Commun.*, vol. 17, no. 5, pp. 3258–3268, May 2018.

[62] C. Geng, N. Naderializadeh, A. S. Avestimehr, and S. A. Jafar, "On the optimality of treating interference as noise," *IEEE Trans. Inf. Theory*, vol. 61, no. 4, pp. 1753–1767, Apr. 2015.

[63] T. L. Marzetta, E. G. Larsson, and H. Yang, *Fundamentals of Massive MIMO*. Cambridge, U.K.: Cambridge Univ. Press, 2016.

Anthony Bardou received the Ph.D. degree from the École Normale Supérieure de Lyon (ENSL). He is a Post-Doctoral Researcher at the INDY Laboratory, EPFL. His research mainly focuses on black-box optimization techniques, kernel methods, online learning, and their applications to develop real-world technological solutions, especially in wireless networking. His work has been recognized by a few Best Paper Awards and the Best Thesis Award from GDR RSD/ACM SIGOPS France.

Jean-Marie Gorce (Senior Member, IEEE) received the M.Sc. and Ph.D. degrees in electrical engineering from the Institut National des Sciences Appliquées (INSA), Lyon, France, in 1993 and 1998, respectively. He was the Co-Founder of the Centre for Innovation, Telecommunications, and Integration of Services (CITI Lab) in 2001. From 2013 to 2014, he was a Visiting Scholar with Princeton University, Princeton, NJ, USA. He has been the Deputy Director of science at INRIA Grenoble Rhône-Alpes from 2017 to 2021 and the Director of science at INRIA Lyon from 2021 to 2024. He is a Professor with INSA de Lyon, and is the Director for Research of Inria, France. He has been involved in several French and European sponsored projects. He has co-published more than 200 conference and journal articles in major venues. His research interests concern multi-user communication systems, with approaches combining information theory, coding, distributed algorithms, signal processing and machine learning. He is currently member of European Project INSTINCT on joint communication and sensing for 6G.

Thomas Begin received the Ph.D. degree in computer science from Sorbonne University, Paris. Following his Ph.D. studies, he completed a Post-Doctoral Fellowship at UC Santa Cruz, USA, in 2009. From 2009 to 2022, he was an Associate Professor at University Lyon 1, France. From 2015 to 2016, he took a research leave at the University of Ottawa, Canada. Since 2022, he has been a Full Professor at University Lyon 1. He is also a co-author of the textbook *Computer Performance Modeling*. He has authored more than 100 articles in international peer-reviewed journals and conference proceedings. His research interests include performance evaluation, computer networks, cloud computing, and system modeling. These interests are primarily applied in high-level modeling, wireless networks, resource allocation, and queueing systems, covering both theoretical and practical aspects. He has been recognized with the two best paper awards and received the ACM MSWiM Rising Star Award in 2020.